JVI
Journals.ASM.org

Viral Interferon Regulatory Factors Are Critical for Delay of the Host Immune Response against Rhesus Macaque Rhadinovirus Infection

Bridget A. Robinson,[a,b] Megan A. O'Connor,[b] He Li,[b] Flora Engelmann,[b] Britt Poland,[c] Richard Grant,[c] Victor DeFilippis,[b] Ryan D. Estep,[b] Michael K. Axthelm,[b,d] Ilhem Messaoudi,[a,b,d] and Scott W. Wong[a,b,d]

Department of Molecular Microbiology and Immunology, Oregon Health & Science University, Portland, Oregon, USA[a]; Vaccine and Gene Therapy Institute, Beaverton, Oregon, USA[b]; SNBL USA, Everett, Washington, USA[c]; and Division of Pathobiology and Immunology, Oregon National Primate Research Center, Beaverton, Oregon, USA[d]

Kaposi's sarcoma-associated herpesvirus (KSHV) and the closely related gamma-2 herpesvirus rhesus macaque (RM) rhadinovirus (RRV) are the only known viruses to encode viral homologues of the cellular interferon (IFN) regulatory factors (IRFs). Recent characterization of a viral IRF (vIRF) deletion clone of RRV (vIRF-knockout RRV [vIRF-ko RRV]) demonstrated that vIRFs inhibit induction of type I and type II IFNs during RRV infection of peripheral blood mononuclear cells. Because the IFN response is a key component to a host's antiviral defenses, this study has investigated the role of vIRFs in viral replication and the development of the immune response during *in vivo* infection in RMs, the natural host of RRV. Experimental infection of RMs with vIRF-ko RRV resulted in decreased viral loads and diminished B cell hyperplasia, a characteristic pathology during acute RRV infection that often develops into more severe lymphoproliferative disorders in immune-compromised animals, similar to pathologies in KSHV-infected individuals. Moreover, *in vivo* infection with vIRF-ko RRV resulted in earlier and sustained production of proinflammatory cytokines and earlier induction of an anti-RRV T cell response compared to wild-type RRV infection. These findings reveal the broad impact that vIRFs have on pathogenesis and the immune response *in vivo* and are the first to validate the importance of vIRFs during *de novo* infection in the host.

Kaposi's sarcoma (KS)-associated herpesvirus (KSHV) is a gamma-2 gammaherpesvirus that was identified in 1994 to be the cause of AIDS-related KS (11), one of the most common malignancies within human immunodeficiency virus (HIV)-infected individuals. KSHV establishes a persistent infection within B cells (2, 14) and is also associated with the malignant B cell disorders, multicentric Castleman's disease (MCD), and primary effusion lymphoma (PEL) (9, 48). Patients who develop MCD and PEL often have a poor outcome, especially if these B cell disorders develop before the introduction of highly active antiretroviral therapy (HAART) (7). Moreover, recent studies have documented an increase in KS within individuals on long-term therapy, despite maintenance of low HIV loads and high CD4 T cell numbers (31). These findings now suggest that the development of KSHV-associated diseases is dependent on other unidentified factors and not simply just immune suppression.

Studying host-pathogen interactions during *de novo* KSHV infection and disease pathogenesis has been hindered by the scarcity of animal models that recapitulate the human disease (10, 16, 42). Rhesus macaque (RM) rhadinovirus (RRV) is a closely related gammaherpesvirus (1, 13, 15, 46) that naturally infects RMs and establishes latency within B cells (4). Moreover, RRV infection of RMs induces an acute hyperproliferation of B cells (17, 54) that often develops into diseases that resemble non-Hodgkin's lymphoma and MCD in immune-compromised animals (37). The striking similarities between KSHV- and RRV-associated pathologies (4, 17, 37, 54), along with the nearly colinear genomic organization (1, 46), make RRV infection of RMs an ideal model for studying KSHV disease. Moreover, recent generation and characterization of a bacterial artificial chromosome (BAC) clone of RRV isolate 17577 (wild-type BAC-derived [WT_{BAC}] RRV_{17577}) (17) allow specific genes to be targeted for deletion to effectively address their roles during infection.

KSHV and RRV encode a number of viral homologues of cellular genes involved in immune signaling, apoptosis, and cellular growth and differentiation. Accordingly, these viral homologues play critical roles in subverting the immune response (3). In particular, KSHV and RRV both encode a cluster of viral interferon (IFN) regulatory factors (vIRFs) (1, 33, 45, 46) which bear significant homology with cellular IRFs, a family of transcription factors that coordinates induction of IFN and other proinflammatory cytokines during virus infection (21). RRV encodes eight vIRFs (open reading frames [ORFs] R6 to R13) within the same genomic region as the 4 vIRFs encoded within KSHV (1, 46). KSHV vIRF-1, -2, and -3 inhibit the induction of IFN and subsequent IFN-induced signaling via direct and indirect interference with cellular IRFs (5, 6, 18–20, 24, 29, 52, 55). Furthermore, KSHV vIRF-1 displayed tumorigenic potential in NIH 3T3 cells and nude mice (20), and KSHV vIRF-1, -3, and -4 independently disrupt p53 function, inhibiting p53-induced apoptosis and/or cell cycle control (28, 34, 43, 47). Additional antiapoptotic functions have also been attributed to KSHV vIRF-1 and vIRF-3. For example, KSHV vIRF-1 binds and sequesters the proapoptotic protein Bim, reducing levels of apoptosis (12), and RNA interference knockdown of KSHV vIRF-3 results in increased activity of effector caspases in KSHV-infected PEL cells (53). Collectively, these data illustrate the functional breadth and diversity of pathways/cellular functions that are targeted by the vIRFs, but these data do not adequately address the role of vIRFs during *in vivo* infection.

Received 13 July 2011 **Accepted** 8 December 2011
Published ahead of print 14 December 2011
Address correspondence to Scott W. Wong, wongs@ohsu.edu.

doi:10.1128/JVI.05657-11

Recent generation of a recombinant clone of RRV lacking all 8 vIRFs (IRF-knockout RRV [vIRF-ko RRV]) demonstrated that RRV vIRFs inhibit the induction of IFN during *de novo* RRV infection in peripheral blood mononuclear cells (PBMCs) and rhesus fibroblasts (RFs) (44). Specifically, infection of PBMCs with vIRF-ko RRV induced significantly more type I IFN (alpha/beta IFN [IFN-α/β]) and type II IFN (IFN-γ) than WT_{BAC} RRV. Moreover, increased production of IFN-α was most evident within plasmacytoid dendritic cells (pDCs), which are also important in Toll-like receptor 9-mediated detection of KSHV (50). Therefore, we hypothesized that vIRF-ko RRV infection of RMs would result in increased induction of IFN, promoting a more effective adaptive immune response and potentially limiting viral replication, persistence, and/or acute RRV-associated pathology. This hypothesis was tested by infecting immunocompetent RMs with either WT_{BAC} RRV or vIRF-ko RRV and comparing viral replication and development of the adaptive immune response. These data show for the first time that vIRFs are critical for efficient viral growth, subversion of early cytokine production, and delay of the T cell response, as well as important in development of acute B cell pathologies during RRV infection in RMs.

MATERIALS AND METHODS

Cells and virus. Primary RFs were grown in Dulbecco modified Eagle medium (Mediatech, Herndon, VA) supplemented with 10% fetal bovine serum (HyClone, Ogden, UT). Viruses used in these studies include wild-type BAC-derived RRV_{17577} (WT_{BAC} RRV) (17) and vIRF-ko RRV_{17577} (vIRF-ko RRV), generated from the WT_{BAC} recombinant virus (44). All virus stocks were purified through a 30% sorbitol cushion and resuspended in phosphate-buffered saline, and titers in RFs were determined using standard plaque assay.

Experimental inoculation of rhesus macaques with BAC-generated WT RRV and vIRF-ko RRV. All aspects of the experimental animal studies were performed according to institutional guidelines for animal care and use at the Oregon National Primate Research Center, Beaverton, OR. Expanded-specific-pathogen-free (ESPF), juvenile RMs, seronegative for RRV, were inoculated intravenously with 5×10^6 PFU. Six RMs were infected with BAC-derived WT_{BAC} RRV (RM identification numbers 24807, 24896, 24996, 24916, 21963, and 26473), and 8 RMs were infected with BAC-derived vIRF-ko RRV (RM identification numbers 24875, 25491, 24799, 25000, 21287, 26448, 26937, and 25241). RM 25241 developed neurological symptoms unrelated to RRV infection at 16 days postinfection (dpi) and underwent necropsy 2 days later, so there are no data for this animal after 14 dpi.

Blood was collected at 1, 3, 5, 7, and 10 dpi and then weekly for the duration of these studies, to obtain PBMCs. Bronchoalveolar lavage (BAL) was also performed weekly to collect infiltrating immune cells in the lung. Preinfection samples were collected 4 and 2 weeks prior to RRV infection, as well as on day 0, to establish baseline readings for each animal. PBMCs were isolated from whole blood using Histopaque (Sigma-Aldrich, St. Louis, MO) per the manufacturer's guidelines.

Viral loads, persistence, and detection of WT or vIRF-ko RRV in RMs. To measure viral loads in the infected RMs, total DNA was isolated from whole blood or sorted $CD20^+$ cells, and genome copies were calculated using TaqMan primers/probe specific for RRV ORF3 (viral macrophage inflammatory protein [vMIP]): primer vMIP-1 (5′-CCTATGGGC TCCATGAGC-3′), primer vMIP-2 (5′-ATCGTCAATCAGGCTGCG-3′), and probe vMIP (5′-TCATCTGCCGCCACCCGGTTTA-3′) as previously described (17).

The presence of infectious virus was measured via coculture of PBMCs, as described previously (17). Briefly, 2×10^5 PBMCs were added in duplicate onto confluent monolayers of RFs and serially diluted 1:3 across a 24-well plate, and the development of cytopathic effect (CPE) was scored (17). A maximum score of 5 indicates that CPE was present at the highest dilution (2.5×10^3 PBMCs/well), and half scores represent CPE in only 1 of the replicate wells at that respective dilution. At peak days of viremia, coculture supernatant/cells were collected and used as template to verify the presence of RRV via nested PCR for RRV ORF3 (vMIP). These analyses utilized the vMIP-1 and vMIP-2 oligonucleotides (see above) for the initial reaction and primers vMIP-3 (5′-CCC GAA CTC TGC TGT TTG-3′) and vMIP-4 (5′-TGGGACGCTTGTCCACCG-3′) for the nested reaction. A fragment within ORF R10 (vIRF) was also amplified using the following oligonucleotides: R10-1 (5′-CGT TTC CCA ATT ATG ATT ATC-3′) and R10-2 (5′-CCG ATA CCG TCT CTC TTG ATC-3′).

To check for persistence of the RRV genome, $CD20^+$ B cells were isolated via fluorescence-activated cell sorting from 5×10^7 PBMCs collected from available animals at 3, 6, 9, and 24 months postinfection. DNA was extracted from $CD20^+$ B cells with a PureGene DNA extraction kit (Qiagen, Valencia, CA), per the manufacturer's protocol, and analyzed via quantitative PCR (qPCR) and nested PCR for RRV ORF3 (vMIP), as described above.

Measurement of T and B cell proliferation. PBMCs and BAL fluid cells were stained for extracellular markers CD8b (Beckman Coulter, Brea, CA) and CD4 (eBioscience, San Diego, CA) to define $CD4^+$ and $CD8^+$ T cell subsets, as well as $CD20^+$ (Biolegend, San Diego, CA), CD27 (eBioscience), and IgD (Southern Biotech, Birmingham, AL) to define naïve, marginal zone (MZ)-like, and memory B cell subsets, as described previously (32). Cells were subsequently fixed and permeabilized per the manufacturer's protocol (BioLegend) and then stained for Ki67 (BD Pharmingen, San Jose, CA), a nuclear antigen involved in DNA replication. Samples were acquired on an LSRII instrument (BD), and data were analyzed using FlowJo software (TreeStar, Ashland, OR). Complete blood counts were obtained to determine peripheral lymphocyte numbers for each RM and used to convert the percentages of Ki67-positive ($Ki67^+$) $CD4^+$ and $CD8^+$ T cells into cell numbers/μl blood. Total lymphocyte counts in the BAL fluid cannot be accurately determined, so the percentages of $Ki67^+$ $CD4^+$ and $CD8^+$ T cells were used. Baseline levels of $Ki67^+$ cells were measured at two time points prior to RRV infection, averaged, and set equal to 1. Levels at subsequent time points were then calculated and expressed as the fold change in the $Ki67^+$ population compared to baseline in each RM.

Intracellular cytokine staining. PBMCs and BAL fluid cells were stimulated overnight with RRV at a multiplicity of infection of 1, followed by 6 h of incubation with brefeldin A (0.02 μg/μl; Sigma) to block cytokine secretion. Anti-CD3 antibody (FN18; Invitrogen Biosource, Carlsbad, CA) and vaccinia virus (VV) were used as a positive and a negative control, respectively. Cells were then stained to define T cell populations using CD8b and CD4, followed by intracellular staining for IFN-γ and tumor necrosis factor alpha (TNF-α). Cells were acquired on an LSRII instrument (BD), and data analysis was carried out using FlowJo software. Final data are represented as the percentage of $CD4^+$ or $CD8^+$ T cells that expressed IFN-γ (the sum of single-positive [IFN-γ^+] and double-positive [IFN-γ^+/TNF-α^+] T cells) after *ex vivo* stimulation with RRV. Nonspecific responses to VV stimulation never exceeded 0.5% of responding cells and were subtracted for each time point.

Measuring serum RRV antibodies. Plasma was collected from RMs weekly, and antiviral IgG levels were measured using a standard enzyme-linked immunosorbent assay (ELISA) with plates coated with optimized amounts of RRV-infected cell lysate. Serial 3-fold dilutions of RM plasma were incubated in triplicate on ELISA plates for 1 h and washed, and signal was detected and quantified using anti-IgG–horseradish peroxidase and chromogen substrate. Log-log transformation of the linear portion of the curve was then performed, and a value of 0.1 optical density unit was used as the cutoff point to calculate endpoint titers. Each plate included a positive-control sample that allowed normalization of ELISA titers between assays and a negative-control sample to ensure the specificity of the assay conditions.

Luminex analysis. To measure cytokines in infected RMs, plasma was collected from blood on 0, 1, 3, 5, 7, and 14 dpi. Twenty-three cytokines were simultaneously measured using a Milliplex nonhuman primate (NHP) 23-plex cytokine kit (Millipore, Billerica, MA). Analysis was performed on a Luminex 100/200 system. Baseline readings of cytokines (pg/ml) in each macaque were measured on 0 dpi and subtracted from the readings at each time point for normalization of the data.

Measuring IFN-α in plasma. Plasma obtained during the first 2 weeks after RRV infection was stored at −80°C until samples from all time points could be assayed simultaneously. To assay for biologically active type I IFN, an IFN-responsive cell line was generated. RFs stably expressing human telomerase (tRFs) (26) were transduced with a replication-defective lentivirus encoding firefly luciferase downstream of an IFN-stimulated response element (ISRE; Qiagen). Transduced tRF-ISRE cell cultures were then purified by exposure to 3 μg/ml puromycin, resistance to which is conferred by the lentivirus.

To normalize luciferase expression, the tRF-ISRE cells were transiently transfected with pRL-SV40 (Promega, Madison, WI) 24 h prior to assay using an Amaxa nucleofection system (kit L, program T-30; Lonza, Cologne, Germany). Plasma was then added to the reporter cells for 6 h, and firefly and *Renilla* luciferase expression was measured using a Dual-glo luciferase assay system (Promega), per the manufacturer's protocol. Data are represented as a ratio of firefly luciferase expression/*Renilla* luciferase expression, and any background signal at 0 dpi was subtracted from data obtained at all subsequent time points. Data were analyzed in a dichotomous format to statistically compare detection of type I IFN (response = 1, no response = 0) in WT_{BAC} and vIRF-ko RRV-infected RMs.

Statistical analysis. Data measuring B cell hyperplasia, T cell responses, and cytokine production were statistically analyzed using GraphPad Instat software (GraphPad Software, La Jolla, CA), with P values of $\leq$0.05 considered significant and P values of from 0.05 to 0.1 considered to be showing a significant trend. Dichotomous data from IFN-α bioassays were compared via logistical regression using the web-based program at http://StatPages.org/logistic.html, which is part of the StatPages.org website, maintained by John C. Pezzullo, Georgetown University, Washington, DC (accessed 20 October 2011); this program implements an algorithm described elsewhere (22). Time (dpi) and virus (vIRF-ko RRV = 1, compared to WT_{BAC} RRV [the reference] = 0) were used as independent variables to determine the odds ratio (OR) of IFN-α production. The OR is a measure of the increase in the dependent variable (e.g., IFN) as the value of the independent value (e.g., dpi) is increased by 1 unit.

RESULTS

Infection of rhesus macaques with vIRF-ko RRV results in lower viral loads and earlier detection of lytic virus. Immunocompetent, ESPF RMs were infected intravenously with 5×10^6 PFU of either WT_{BAC} RRV ($n = 6$) or vIRF-ko RRV ($n = 8$). The infected RMs were monitored for 10 weeks postinfection (p.i.) to assess viral loads by qPCR, lymphocyte proliferation, anti-RRV T cell and antibody responses, and changes in plasma cytokine levels. RRV DNA was initially detected at 14 dpi in 3 animals, and viral loads peaked at 28 dpi in all 6 WT_{BAC} RRV-infected RMs (Fig. 1A). In contrast, viral loads in 6 of the 8 RMs infected with vIRF-ko RRV remained below the level of detection for this qPCR assay during the entire study (Fig. 1B). Interestingly, the remaining 2 vIRF-ko RRV-infected animals (RMs 21287 and 25241) presented with quantifiable viral loads at 7 dpi (Fig. 1B). And although peak viral loads were much lower in animals infected with vIRF-ko RRV, the measurable viral loads were detected 1 to 2 weeks earlier than in RMs infected with WT_{BAC} RRV (Fig. 1A and B).

Coculture methods were utilized to measure infectious virus and verify the presence of RRV. PBMCs from infected RMs were serially diluted and cocultured with RFs weekly, monitored for CPE, and subsequently given a viremic score (a viremic score of 0 represents no CPE in any wells, and a score of 5 represents CPE in replicate wells at the highest dilution of PBMCs). Viremia was detected at 21 dpi and peaked at 28 dpi in all WT_{BAC} RRV-infected RMs (Fig. 1C), which correlated with peak viral loads in those animals (Fig. 1A). Although genome equivalents were below the limit of detection by qPCR in 6 of the vIRF-ko RRV-infected animals (Fig. 1B), infectious virus was detected via coculture in 7 of these animals, with peak viremic scores occurring at between 7 and 14 dpi (Fig. 1D). Therefore, coculture methods detected infectious virus 2 weeks earlier than in WT_{BAC} RRV-infected animals (Fig. 1C), which also correlated with earlier measurement of viral loads in 2 of the vIRF-ko RRV-infected animals at 7 to 14 dpi (Fig. 1B).

When coculture wells reached full CPE on 14 and 28 dpi for the vIRF-ko and WT_{BAC} RRV-infected animals, respectively, cells and supernatant were collected and subjected to PCR analyses to verify the presence of RRV and differentiate between WT_{BAC} and vIRF-ko RRVs. Nested PCR of the sequence within RRV ORF3 (vMIP) verified that infectious virus recovered from the infected RMs was RRV (Fig. 1E), and a second PCR analysis distinguished WT RRV from vIRF-ko RRV via amplification of a region within ORF R10 (vIRF), confirming that the vIRF-ko RRV-infected animals received only the recombinant virus (Fig. 1E).

The vIRFs are important for the induction of the characteristic B cell hyperplasia during acute RRV infection. Acute B cell hyperplasia is a defining form of pathology observed early during RRV infection (17, 37, 54). In these studies, all 6 WT_{BAC} RRV-infected RMs developed B cell hyperplasia between 28 and 42 dpi, with peak numbers of $CD20^+$ B cells averaging 6-fold higher than those on day 0 (Fig. 2A). Furthermore, after this initial proliferative burst, WT_{BAC} RRV-infected RMs continued to maintain a higher baseline of total $CD20^+$ cells at 56 and 63 dpi compared to levels prior to infection ($P \leq 0.002$) (Fig. 2A). In contrast, the vIRF-ko-infected RMs experienced only a modest increase (~2-fold) in total $CD20^+$ B cells, with peak numbers being significantly lower ($P \leq 0.05$) than those in WT_{BAC} RRV-infected RMs (Fig. 2A).

To further characterize the $CD20^+$ population during this hyperplastic phase, the proliferative burst within naïve ($CD27^-$, IgD-positive [IgD^+]), marginal zone (MZ)-like ($CD27^+$, IgD^+), and memory ($CD27^+$, IgD-negative [IgD^-]) B cell populations was measured via changes in the expression of the proliferation marker Ki67 (41). Upon antigen encounter, naïve B cells simultaneously acquire memory markers and begin a robust proliferative burst. In WT_{BAC} RRV-infected RMs, the increase in total $CD20^+$ B cells coincided with a distinct increase in $Ki67^+$ memory B cells (Fig. 2B), but there were no obvious proliferative bursts within naïve or MZ-like B cell populations (data not shown). Thus, these observations suggest that B cell hyperplasia is driven by naïve B cells converting into memory B cells and/or potential bystander proliferation of memory B cells. Not surprisingly, there was a less significant increase in $Ki67^+$ B cells in the vIRF-ko RRV-infected RMs (Fig. 2B and data not shown), which is in accordance with the lack of B cell hyperplasia in these animals.

Deletion of the vIRFs decreases levels of persistent RRV. To examine whether deletion of the vIRFs inhibits RRV persistence in these RMs, purified B cells ($CD20^+$), the main site of viral persistence (4), were analyzed via qPCR to quantify the prevalence of RRV genomes at 3, 6, 9, and 24 months p.i. (Fig. 3A). WT_{BAC} RRV

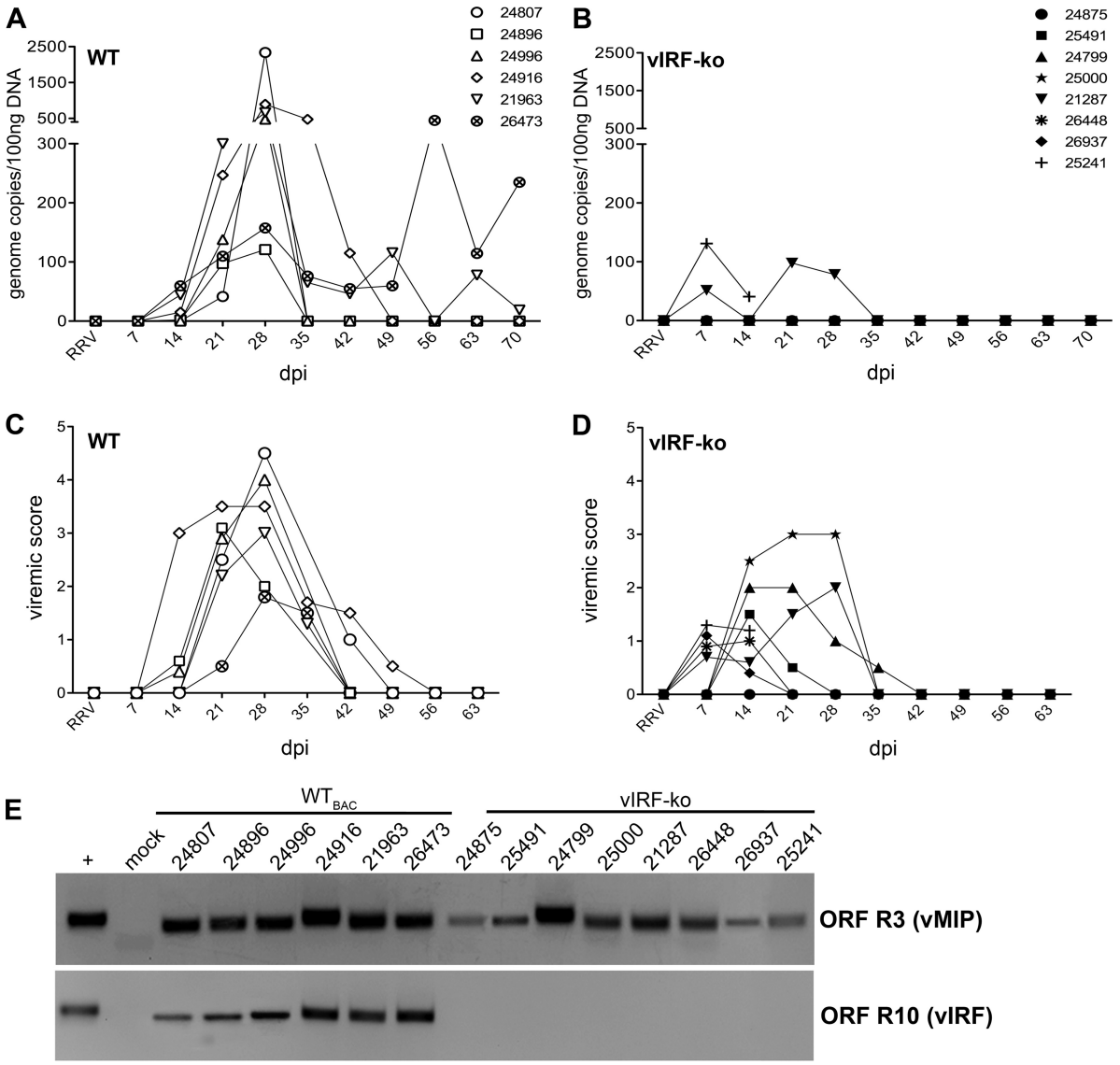

FIG 1 Detection of RRV DNA and lytic replication measured in RRV-infected RMs. Expanded-specific-pathogen-free RMs were infected intravenously with 5×10^6 PFU of WT_{BAC} RRV ($n = 6$) or vIRF-ko RRV ($n = 8$). Each RM is labeled with an identifying number and an individual symbol. (A and B) Whole blood was analyzed weekly via qPCR to determine RRV loads. Data are represented as number of RRV genome copies/100 ng DNA in each of the WT_{BAC} RRV-infected RMs (A) and the vIRF-ko RRV-infected RMs (B). (C and D) PBMCs (2×10^5) were cocultured with confluent RFs and serially diluted (1:3) across a 24-well plate. Viremic score correlates with the highest dilution of PBMCs that resulted in CPE when cocultured with RFs. A viremic score of 5 indicates the presence of CPE in wells with the highest dilution of PBMCs (2.5×10^3 PBMCs), and the presence of CPE in duplicate wells at each dilution has a viremic score of 0.5. (E) The presence of RRV DNA in cocultures was verified via nested PCR using primers for RRV ORF R3 (vMIP), as well as RRV ORF R10 (vIRF), to differentiate WT and vIRF-ko RRV.

was consistently detected at 3 and 6 months p.i. and in 2 of the 3 RMs tested at 9 months p.i. (Fig. 3A). At 2 years p.i., however, persistent virus was below the level of detection by qPCR methods (Fig. 3A), but nested PCR analyses verified that RRV was still present within these animals (RMs 24896 and 24996) (Fig. 3B). Levels of persistent virus in the vIRF-ko RRV-infected RMs were below the detection limits of qPCR at all time points tested (Fig. 3A), but RRV genomes were detected via nested PCR, suggesting that RRV is persisting in these animals (Fig. 3B). Therefore, these analyses confirmed the presence of RRV genomes within $CD20^+$ B cells in both WT_{BAC} and vIRF-ko RRV-infected RMs, albeit at much lower levels following vIRF-ko RRV infection.

Reduced T cell proliferation after infection with vIRF-ko RRV. T cells typically undergo a burst of proliferation following antigenic stimulation, which can be assessed by measuring changes in the frequency of $Ki67^+$ cells (32). PBMCs were analyzed weekly to measure the kinetics and the magnitude of the $CD4^+$ and $CD8^+$ T cell proliferative response (Fig. 4). T cell proliferation was detected in the blood of both WT_{BAC} and vIRF-ko RRV-infected RMs at 14 dpi, peaked at between 28 and 35 dpi, and contracted by 49 dpi in both CD4 (Fig. 4A) and CD8 (Fig. 4B) subsets. Overall, however, T cell proliferation within the blood was less robust in the animals infected with vIRF-ko RRV (Fig. 4A and B). Simultaneously, proliferative T cell responses were also

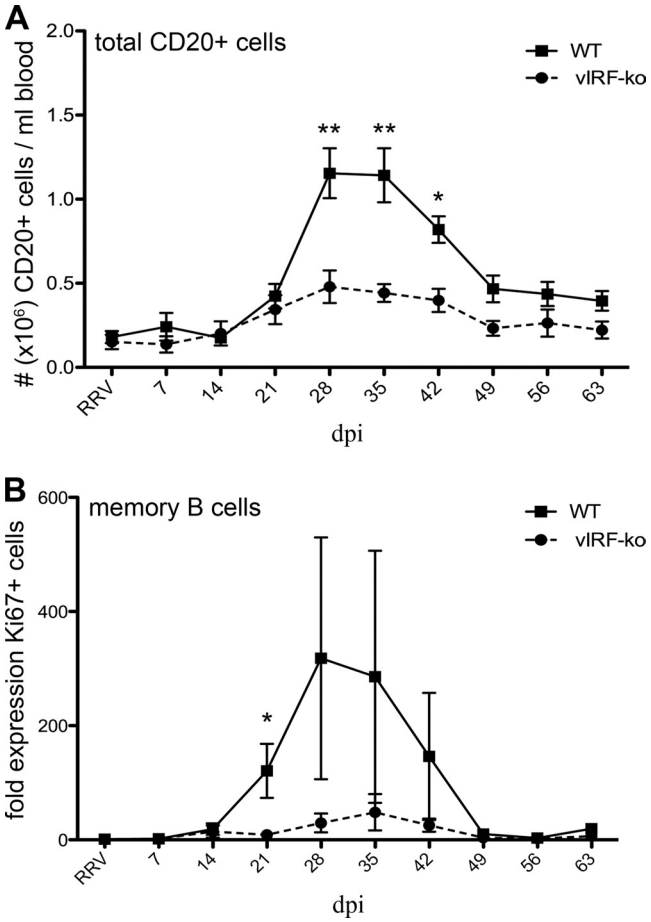

FIG 2 Decreased B cell hyperplasia in vIRF-ko RRV-infected RMs. (A) Absolute numbers of $CD20^+$ cells were calculated by converting the percentage of $CD20^+$ lymphocytes using the total number of lymphocytes/ml blood obtained via a complete blood count machine (Hemavet). Data are represented as absolute number (10^6) of $CD20^+$ cells/ml peripheral blood and are averaged (± SEM) among the WT RRV-infected cohort ($n = 6$) and the vIRF-ko RRV-infected cohort ($n = 8$). (B) The average (± SEM) frequency of $Ki67^+$ memory B cells was calculated for WT_{BAC} and vIRF-ko RRV-infected animals as described for panel A, and the baseline (preinfection) $Ki67^+$ population was set equal to 1. Data were analyzed using an unpaired Student's *t* test. **, $P \leq 0.01$; *, $P \leq 0.05$.

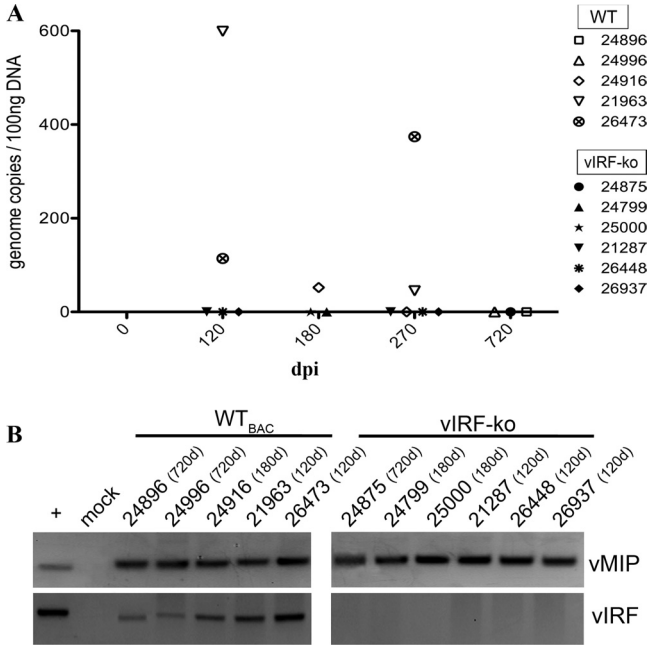

FIG 3 Lower levels of viral persistence in vIRF-ko RRV-infected RMs. The presence of RRV genomic DNA within $CD20^+$ cells was analyzed between 3 and 24 months postinfection. $CD20^+$ B cells were sorted from PBMCs, DNA was extracted, and real-time qPCR (A) and nested PCR (B) analyses were performed to detect RRV ORF R3 (vMIP) and ORF R10 (vIRF).

analyzed in the lung via BAL. Proliferation of CD4 and CD8 T cells was more temporally distinct in the BAL fluid than in the blood (Fig. 4C and D). There was a marked increase in $Ki67^+$ cells in the BAL fluid at 35 dpi in both WT_{BAC} and vIRF-ko RRV-infected animals, suggesting that these were proliferating cells that were trafficking from the blood and not proliferating within the lung (Fig. 4C and D). Moreover, similar to responses in the blood, the level of T cell proliferation in the BAL fluid of vIRF-ko-infected animals was slightly lower than that in the BAL fluid of WT_{BAC} RRV-infected animals (Fig. 4C and D).

Frequency of RRV-specific T cells is higher in the absence of vIRFs. To further characterize the T cell response, the frequency of RRV-specific CD4 and CD8 T cells was measured by intracellular cytokine staining following *ex vivo* stimulation with RRV. Due to blood volume constraints, not every animal could be evaluated at all the time points.

Within the PBMCs, RRV-specific CD4 T cells were detected 7 to 14 days earlier in vIRF-ko RRV-infected RMs than WT_{BAC} RRV-infected animals (Fig. 5A to C). Specifically, 5 of the 6 vIRF-ko RRV-infected RMs analyzed had a measurable CD4 response in the blood at 7 dpi (Fig. 5A and C), whereas none of the WT_{BAC} RRV-infected RMs had a measurable response at 7 dpi ($P = 0.03$) (Fig. 5A and B). Similarly, the CD8 response in the blood was also initiated at 7 dpi in the vIRF-ko RRV-infected RMs (Fig. 5A and E), while WT_{BAC} RRV-infected animals did not develop a median CD8 response in the blood until 21 dpi (Fig. 5A and D). Although there were minimal T cell responses in the blood after 28 dpi, RRV-specific T cells persisted in BAL fluid cells, with 2 to 4% of CD4 T cells and 3 to 6% of CD8 T cells responding to RRV stimulation throughout the course of these studies; however, there were no significant differences in maintenance of the T cell response between WT_{BAC} and vIRF-ko RRV infection (data not shown). Overall, in comparison to WT_{BAC} RRV infection, there is earlier initiation of the anti-RRV T cell response in vIRF-ko RRV-infected RMs, most notably at 7 dpi (CD4, $P = 0.03$; CD8, $P = 0.07$) (Fig. 5A).

Similar antibody response in WT_{BAC} RRV- and vIRF-ko RRV-infected RMs. To determine whether the RRV antibody response was also influenced by the vIRFs, plasma was collected weekly and assayed using an anti-RRV IgG ELISA. Interestingly, despite earlier detection of RRV via qPCR (Fig. 1B), earlier detection of lytic replication in cocultures (Fig. 1D), and earlier T cell responses in the vIRF-ko RRV-infected RMs (Fig. 5), the anti-RRV IgG response in these animals displayed similar kinetics and magnitude as the response in the WT_{BAC} RRV-infected RMs (Fig. 6). Peak antibody titers were reached at approximately 35 dpi and maintained throughout 63 dpi in all the RMs in this study.

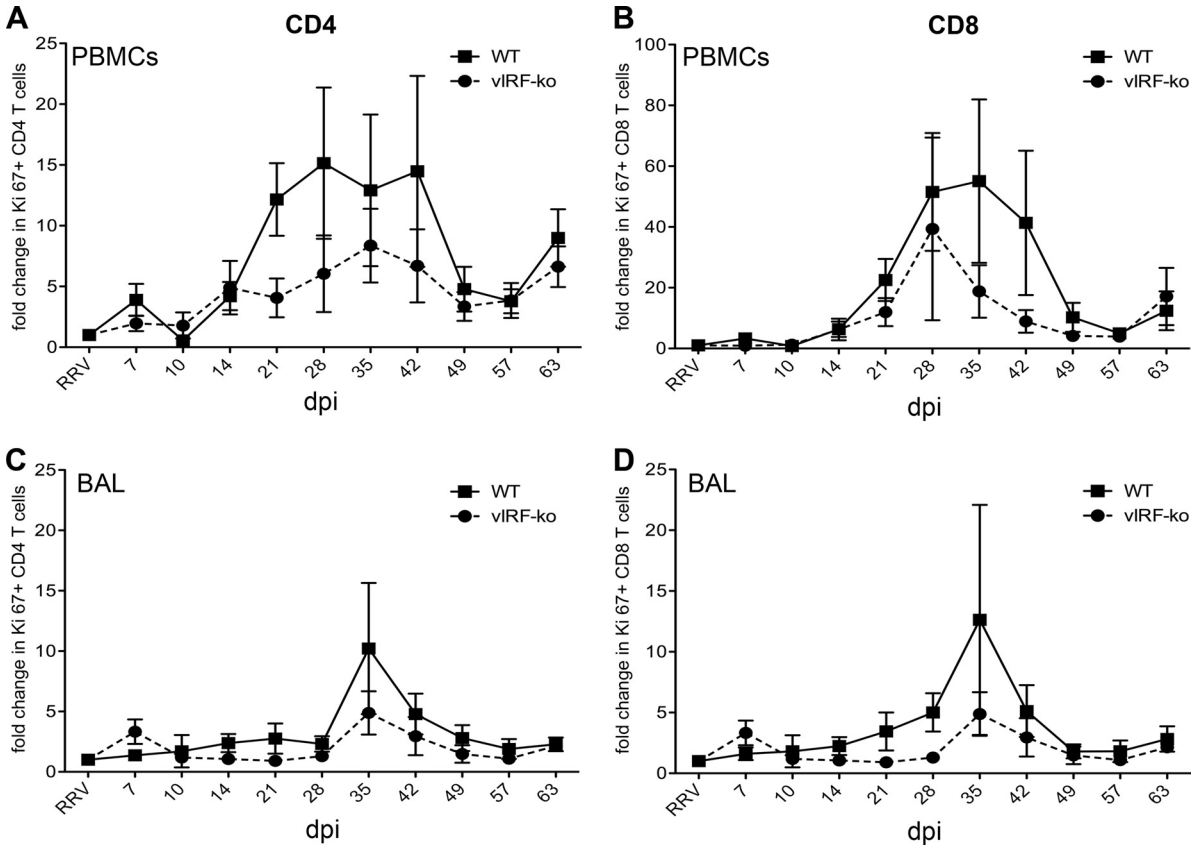

FIG 4 CD4 and CD8 T cell proliferation in peripheral blood and bronchoalveolar lavage fluid. The frequency of proliferating ($Ki67^+$) CD4 and CD8 T cells within PBMCs (A and B) and BAL fluid cells (C and D) was determined by flow cytometry. Preinfection samples were used to establish a baseline, and the fold change in $Ki67^+$ populations in each animal was calculated for each time point. Data are presented as an average (± SEM) of the WT_{BAC} RRV-infected RMs and the vIRF-ko RRV-infected RMs.

vIRFs disrupt early cytokine production during *de novo* RRV infection. The adaptive immune response is greatly influenced by the innate immune response. Therefore, innate cytokine production was assayed by measuring plasma levels of several key cytokines using a nonhuman primate (NHP)-specific Luminex kit. Of the 23 cytokines measured, only 12 were present at quantifiable levels after RRV infection: granulocyte colony-stimulating factor, interleukin-13 (IL-13), IL-15, IL-17, monocyte chemoattractant protein 1, transforming growth factor α, IL-12/23p40, IL-18, IFN-γ, IL-1ra, soluble CD40 ligand, and IL-8 (Fig. 7 and data not shown). Regardless of vIRFs, RRV infection resulted in an increase in plasma levels of most measured cytokines at 1 dpi (Fig. 7 and data not shown). However, two important Th1-related cytokines were differentially expressed in WT_{BAC} and vIRF-ko RRV-infected RMs (Fig. 6). Specifically, plasma levels of IFN-γ quickly peaked at 1 dpi in both groups, but detectable levels of IFN-γ were maintained through the first 7 days only in the vIRF-ko RRV-infected animals (Fig. 7A and B). Additionally, vIRF-ko RRV infection also resulted in an earlier IL-12p40 response (1 dpi) than WT_{BAC} RRV infection (14 dpi) (Fig. 7C and D). Another important Th1-related cytokine, IL-18, was detected with similar kinetics and magnitude in both WT_{BAC} and vIRF-ko RRV-infected animals (Fig. 6E and F). These data suggest a role for vIRFs in inhibiting early and sustained production of IFN-γ and IL-12p40 following RRV infection in the RM.

vIRFs inhibit production of IFN-α after RRV infection. In recent comparisons of WT_{BAC} RRV and vIRF-ko RRV, it was demonstrated that vIRFs play a role in inhibiting production of type I IFN during *de novo* RRV infection, particularly in plasmacytoid dendritic cells (pDCs) (44). Therefore, to determine whether the vIRFs effectively inhibited IFN production during *in vivo* infection in the RMs, we developed a type I IFN-responsive cell line to assay for the presence of biologically active IFN in the plasma of the infected RMs.

Telomerized rhesus fibroblasts (tRFs) were generated to stably express firefly luciferase under the control of an IFN-stimulated response element (ISRE) in the promoter, tRF-ISRE cells. To standardize luciferase readings, tRF-ISRE cells were also transiently transfected with a plasmid constitutively expressing *Renilla* luciferase 24 h prior to addition of RM plasma. To normalize IFN-α responses in each animal, any background response measured at 0 dpi was subtracted from the response at all subsequent time points. Type I IFN production was detected in 6 of the 8 vIRF-ko RRV-infected RMs at 1 dpi, and all 8 animals displayed a sustained response ($\geq$2 consecutive days) within the first 2 weeks p.i. (Fig. 8B). Conversely, type I IFN production was never detected in more than 3 WT_{BAC} RRV-infected RMs at any time point, and only 2 animals (RMs 24896 and 26473) had sustained responses in the first 2 weeks p.i. (Fig. 8A). Due to the arbitrary units of measure for detection of type I IFN, these data were analyzed via lo-

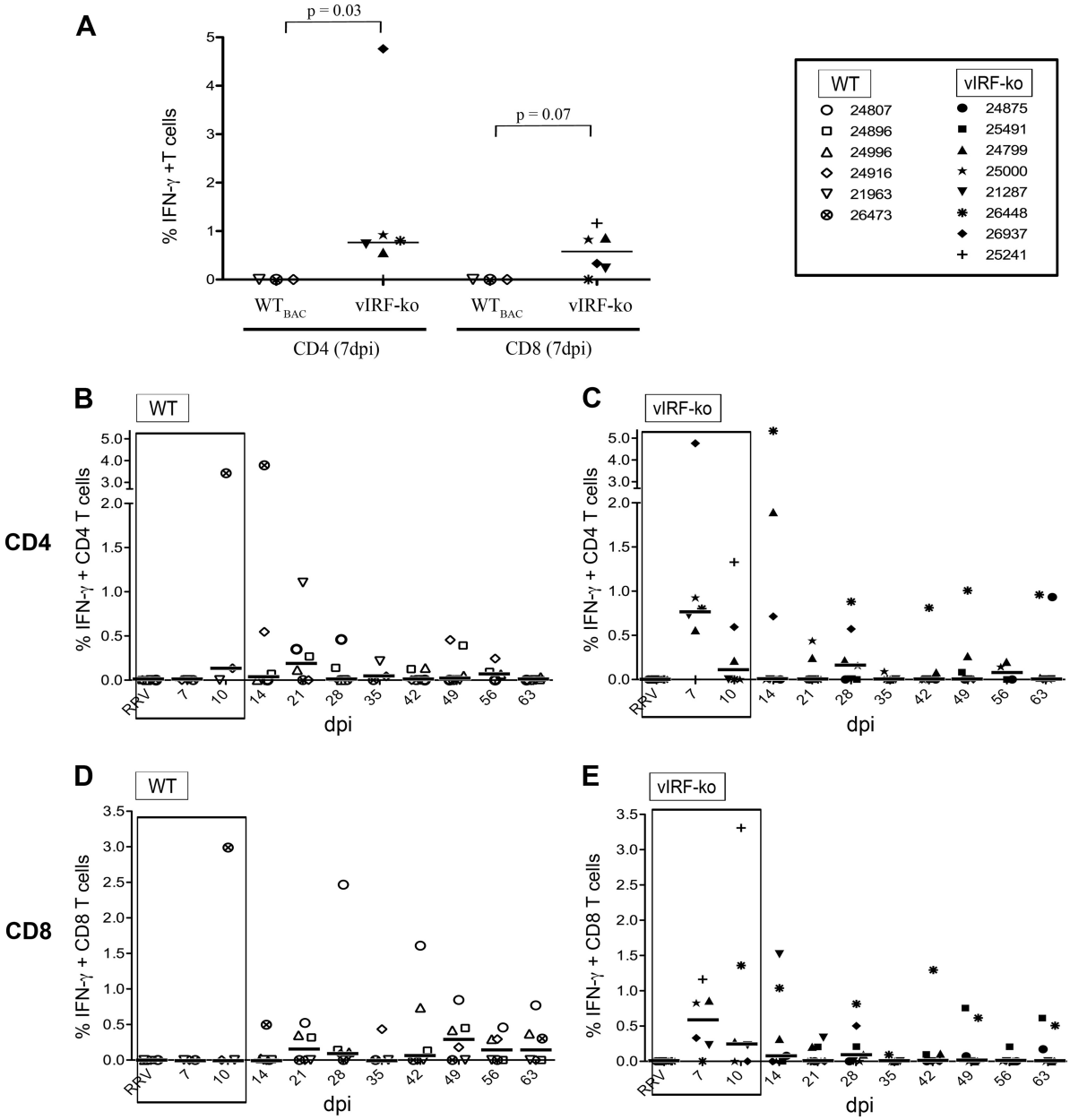

FIG 5 Infection of RMs with vIRF-ko RRV initiates an earlier RRV-specific T cell response. The frequency of RRV-specific T cells within PBMCs was determined after *ex vivo* stimulation with RRV overnight, followed by surface staining for CD4 and CD8 and intracellular cytokine staining for IFN-γ and TNF-α. IFN-γ single-positive (IFN-γ^+) and double-positive (IFN-γ^+/TNF-α^+) cells are added into the final, calculated response. (A) Responses measured at 7 dpi in CD4 and CD8 T cells were compared via unpaired *t* test. (B to E) T cell responses measured during the first 63 dpi are represented in graphs containing data from WT_{BAC} RRV-infected RMs on the left (B and D) and graphs containing data from vIRF-ko RRV-infected RMs on the right (C and E). Data are presented as percentage of RRV-responsive T cells, with baseline and nonspecific (VV) responses subtracted. Median responses are displayed as horizontal lines at each time point. Early time points are boxed to indicate statistical trends and significance and are identical to the data shown in panel A.

gistical regression (no response = 0, response = 1). Using time (dpi) and virus (WT_{BAC} RRV = 0 [reference], vIRF-ko RRV = 1) as independent variables, the probability of detecting type I IFN was found to increase by a factor of 1.17 for each increasing day after RRV infection, regardless of vIRFs ($P = 0.0085$; OR, 1.17; 95% confidence interval [CI], 1.04 to 1.32). More importantly, animals infected with vIRF-ko RRV are 5 times more likely to produce type I IFN than RMs infected with WT_{BAC} RRV ($P = 0.0014$; OR, 5.07; 95% CI, 1.87 to 13.72). These data suggest that the vIRFs significantly inhibit the induction of type I IFN following *de novo* RRV infection in the RM.

DISCUSSION

Herpesviruses have evolved a number of strategies to overcome the innate immune response and evade the subsequent adaptive response (3, 49) in order to initiate a productive infection and

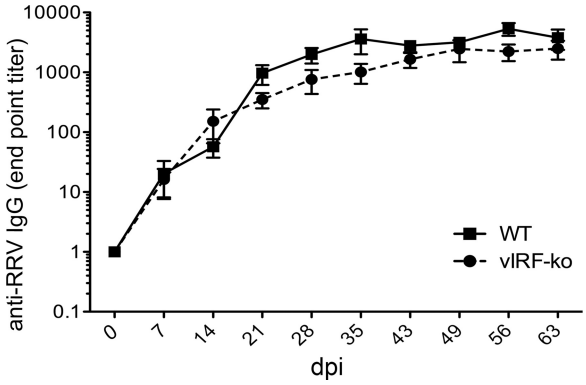

FIG 6 Anti-RRV IgG responses in RMs infected with WT_{BAC} RRV or vIRF-ko RRV. IgG endpoint titers in the plasma were determined using an RRV-specific ELISA. Data are represented as an average (± SEM) of WT_{BAC} RRV-infected RMs ($n = 6$) and vIRF-ko RRV-infected RMs ($n = 8$).

establish latency. These immune evasion strategies include disruption of the IFN response, cytokine/chemokine production and signaling, as well as interference with antigen processing and presentation. KSHV and RRV, in particular, are equipped with a set of unique immune evasion molecules, including vIRFs (35). The data presented here demonstrate an inhibitory role for vIRFs in development of the immune response during primary RRV infection in the RM.

WT_{BAC} and vIRF-ko RRVs share similar growth kinetics *in vitro* (44); however, the significant reduction in viral loads detected following vIRF-ko RRV infection of RMs clearly establishes a critical role for vIRFs during RRV infection *in vivo*. Despite the overall trend of lower viral loads following vIRF-ko RRV infection, we were able to detect RRV DNA in 2 RMs at 7 dpi, which was 1 to 2 weeks earlier than that following WT_{BAC} RRV infection (Fig. 1) (37). Likewise, detection of infectious virus in the vIRF-ko RRV-infected RMs also peaked 2 weeks earlier. This demonstrates that deletion of vIRFs did not completely inhibit viral replication in the RMs, but rather that vIRF-ko RRV infection results in earlier lytic replication that is quickly brought under control, never reaching the same magnitude as in WT_{BAC} RRV infection. There are potentially multiple reasons for the differences in viral loads and lytic replication. One likely reason is that early and maintained production of type I IFN in the absence of vIRFs induces an antiviral state that efficiently inhibits vIRF-ko RRV replication

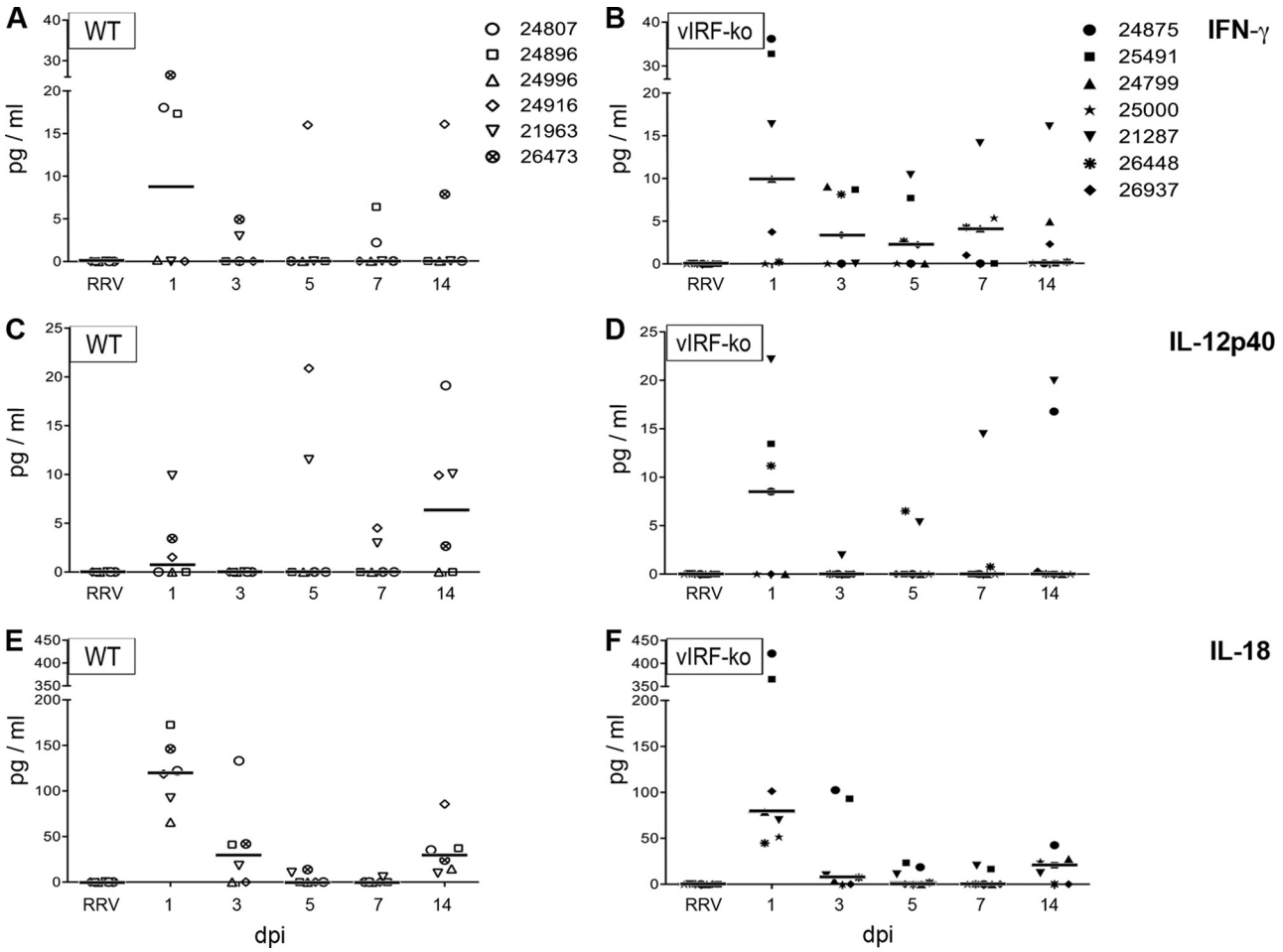

FIG 7 Cytokine levels in the plasma of RRV-infected RMs. Plasma cytokine levels were measured using a rhesus macaque-specific Milliplex kit: IFN-γ (A and B), IL-12p40 (C and D), and IL-18 (E and F). Cytokine responses measured prior to infection were subtracted from the responses at subsequent time points, and data are graphed as pg/ml, with median responses represented as horizontal bars at each time point. WT_{BAC} RRV-infected RMs are graphed on the left, and vIRF-ko RRV-infected RMs are graphed on the right.

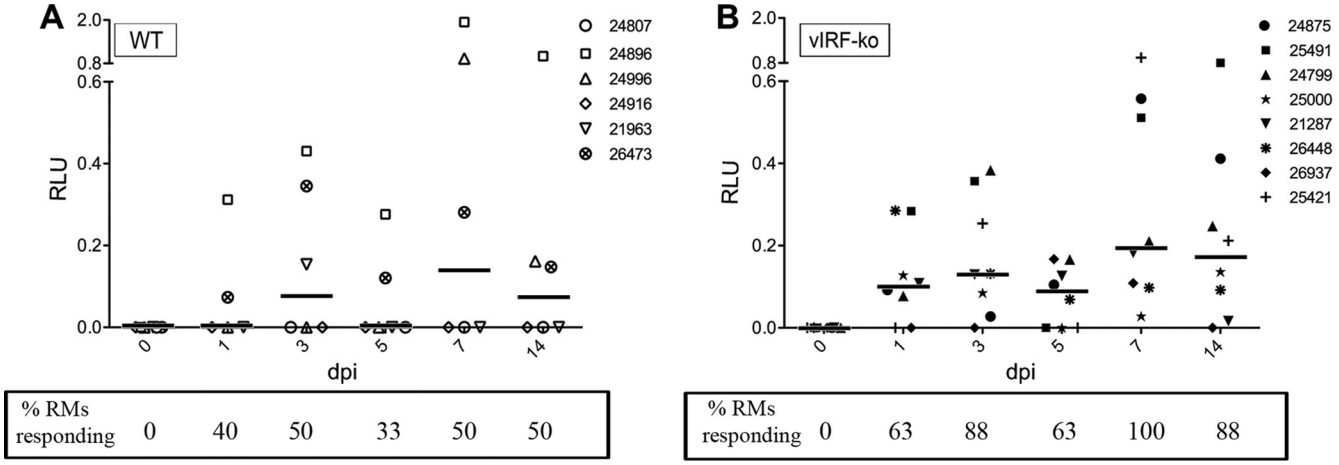

FIG 8 Measuring biologically active type I IFN in the plasma of RRV-infected RMs. Biologically active IFN-α was measured in plasma from WT_{BAC} RRV-infected RMs (A) or vIRF-ko RRV-infected RMs (B) using a luciferase reporter assay. At the time points indicated, plasma was added to cells constitutively expressing firefly luciferase under an ISRE promoter, tRF-ISRE. Baseline readings (preinfection) were subtracted from readings at all subsequent time points. Data were normalized to constitutively expressed *Renilla* luciferase. The number of animals with measured IFN responses was calculated at each time point, and the dichotomous data set (no response = 0, response = 1) was compared using logistical regression. Using responses from the WT_{BAC} RRV-infected animals as the reference (WT = 0, vIRF-ko = 1), virus ($P = 0.0014$; OR, 5.07; 95% CI, 1.87 to 13.72) and dpi ($P = 0.0085$; OR, 1.17; 95% CI, 1.04 to 1.32) were set as independent variables. ISRE, interferon-stimulated response element; RLU, relative luciferase units.

and limits viral spread. In fact, all of the vIRF-ko RRV-infected RMs generated a sustained IFN-α response in the first 14 dpi, whereas only 2 of the WT_{BAC} RRV-infected RMs (RMs 24896 and 26473) showed sustained type I IFN production. Interestingly, RMs 24896 and 26473 also exhibited lower viral loads than the other WT_{BAC} RRV-infected animals, which illustrates that type I IFN production may help to control viral loads. Similarly, IFN-α production by pDCs was significantly higher following *in vitro* infection with vIRF-ko RRV than WT_{BAC} RRV infection (44). Alternatively, earlier detection of lytic replication and decreased viral loads in vIRF-ko RRV-infected RMs could be due to the reduced ability of this virus to inhibit apoptosis. An increase in apoptosis would increase clearance of RRV-infected cells and effectively limit the detection of viral DNA. This hypothesis is supported by the observations that KSHV vIRF-1 and vIRF-3 have antiapoptotic functions necessary for lytic viral production (12) and for *in vitro* survival of KSHV-infected PEL cells, respectively (53). A third possibility is that the vIRFs are important for driving transcription of viral immune modulation genes needed to promote viral replication, as has been shown by the ability of KSHV vIRF-1 to drive transcription of viral IL-6 (vIL-6) (39). Therefore, it is likely that, along with inhibition of IFN, the RRV vIRFs are also targeting apoptotic signaling and viral gene transcription, which would collectively disrupt viral replication in the RM. These possibilities will need to be individually addressed in future studies.

An earlier induction of the anti-RRV T cell response was also detected in vIRF-ko RRV-infected RMs and may also be contributing to decreased viral loads. Additionally, the increased IFN-α levels in the vIRF-ko RRV-infected animals may serve to directly enhance the development and/or maintenance of memory T cells (23). Moreover, IFN-α can also enhance differentiation and activation of DCs (30), thereby promoting antigen presentation in the vIRF-ko RRV-infected RMs. Alternatively, earlier T cell responses in the vIRF-ko RRV-infected animals may be mediated by direct vIRF modulation of antigen presentation. Indeed, previous studies have shown that KSHV vIRF-1 plays a role in inhibiting IFN-γ-induced expression of major histocompatibility complex class I (27). Moreover, data presented here and elsewhere show that RRV vIRFs also act upstream by inhibiting the production of IFN-γ (Fig. 6) (44), a key cytokine in an effective Th1 immune response. Likewise, the cytokine data presented here imply that the vIRFs may also be inhibiting the induction of IL-12, another pivotal cytokine in the development of an antiviral adaptive immune response. Therefore, these data suggest that deletion of vIRFs results in increased and sustained type I IFN and Th1 cytokine production, which collectively could orchestrate a more efficient T cell response in the vIRF-ko RRV-infected RMs.

Deletion of the vIRFs resulted in significantly decreased B cell hyperplasia, a hallmark of RRV infection (37). One reason for the reduced B cell hyperplasia may be decreased viral loads in the vIRF-ko RRV-infected animals. However, the comparable anti-RRV IgG response in WT_{BAC} and vIRF-ko RRV-infected RMs suggests that the hyperplastic B cells are not all RRV specific. Indeed, B cell hyperplasia is thought to be driven by vIL-6, a functional homologue of its cellular counterpart (25, 36–38). Previous studies showed that KSHV vIRF-1 can bind to the KSHV vIL-6 promoter and drive its transcription in latently infected PEL cells *in vitro* (39). Therefore, if vIL-6 expression is even partially controlled by a vIRF(s) during RRV infection, this may be contributing to the decreased B cell hyperplasia following vIRF-ko RRV infection.

The cooperative effect of increased production of type I IFN, an earlier T cell response, and restricted viral replication following acute vIRF-ko RRV infection may also indicate increased control upon RRV reactivation. WT RRV-infected RMs exhibit increased RRV loads following an immune-suppressive event (e.g., simian immunodeficiency virus infection), and higher viral loads often correlate with development of non-Hodgkin's lymphoma or other lymphoproliferative disorders, resembling multicentric Castleman's disease (37). Although RRV was detected in all the animals at between 3 and 24 months p.i. via nested PCR, the quan-

tified level of virus in vIRF-ko RRV-infected animals was never within the limits of detection, suggesting much lower levels of persistence in the absence of the vIRFs. The lower levels of persistent virus in the vIRF-ko RRV-infected RMs could signal better control of reactivation following immune suppression and, in conjunction with a superior immune response, may result in decreased viral shedding and transmission. RRV and KSHV can be readily detected in the saliva of infected RMs (51) and humans (8, 40), respectively, and natural transmission likely occurs at mucosal surfaces. Thus, since intravenous vIRF-ko RRV infection resulted in such a dramatic reduction of viral loads, it is possible that the vIRFs would be even more crucial for transmission and infection at mucosal surfaces, which are natural immunological barriers. Therefore, future analyses will examine if the vIRFs are in fact essential for mucosal infection, reactivation of RRV, and development of disease following subsequent immune suppression.

In summary, the findings presented here establish the broad impact that vIRFs have on the immune response and pathogenesis during *in vivo* RRV infection. Further characterization of the molecular functions of RRV vIRFs will provide insight into novel antiviral therapies and advance our understanding of host-pathogen interactions during KSHV infection.

ACKNOWLEDGMENTS

We thank Lori Boshears for assistance with the manuscript and Byung Park for assistance with statistical analysis.

This work was supported by Public Health Service grants RR00163, RR018107 (M.K.A.), CA75922 (S.W.W.), and CA132638 (S.W.W.). Bridget Robinson was supported by training grant T32 AI07472.

REFERENCES

1. **Alexander L, et al.** 2000. The primary sequence of rhesus monkey rhadinovirus isolate 26-95: sequence similarities to Kaposi's sarcoma-associated herpesvirus and rhesus monkey rhadinovirus isolate 17577. J. Virol. **74**:3388–3398.
2. **Ambroziak JA, et al.** 1995. Herpes-like sequences in HIV-infected and uninfected Kaposi's sarcoma patients. Science **268**:582–583.
3. **Areste C, Blackbourn DJ.** 2009. Modulation of the immune system by Kaposi's sarcoma-associated herpesvirus. Trends Microbiol. **17**:119–129.
4. **Bergquam EP, Avery N, Shiigi SM, Axthelm MK, Wong SW.** 1999. Rhesus rhadinovirus establishes a latent infection in B lymphocytes in vivo. J. Virol. **73**:7874–7876.
5. **Burysek L, et al.** 1999. Functional analysis of human herpesvirus 8-encoded viral interferon regulatory factor 1 and its association with cellular interferon regulatory factors and p300. J. Virol. **73**:7334–7342.
6. **Burysek L, Yeow WS, Pitha PM.** 1999. Unique properties of a second human herpesvirus 8-encoded interferon regulatory factor (vIRF-2). J. Hum. Virol. **2**:19–32.
7. **Carbone A, Cesarman E, Spina M, Gloghini A, Schulz TF.** 2009. HIV-associated lymphomas and gamma-herpesviruses. Blood **113**:1213–1224.
8. **Casper C, et al.** 2007. Frequent and asymptomatic oropharyngeal shedding of human herpesvirus 8 among immunocompetent men. J. Infect. Dis. **195**:30–36.
9. **Cesarman E, Chang Y, Moore PS, Said JW, Knowles DM.** 1995. Kaposi's sarcoma-associated herpesvirus-like DNA sequences in AIDS-related body-cavity-based lymphomas. N. Engl. J. Med. **332**:1186–1191.
10. **Chang H, et al.** 2009. Non-human primate model of Kaposi's sarcoma-associated herpesvirus infection. PLoS Pathog. **5**:e1000606.
11. **Chang Y, et al.** 1994. Identification of herpesvirus-like DNA sequences in AIDS-associated Kaposi's sarcoma. Science **266**:1865–1869.
12. **Choi YB, Nicholas J.** 2010. Bim nuclear translocation and inactivation by viral interferon regulatory factor. PLoS Pathog. **6**:e1001031.
13. **Damania B, Desrosiers RC.** 2001. Simian homologues of human herpesvirus 8. Philos. Trans. R. Soc. Lond. B Biol. Sci. **356**:535–543.
14. **Decker LL, et al.** 1996. The Kaposi sarcoma-associated herpesvirus (KSHV) is present as an intact latent genome in KS tissue but replicates in the peripheral blood mononuclear cells of KS patients. J. Exp. Med. **184**:283–288.
15. **Desrosiers RC, et al.** 1997. A herpesvirus of rhesus monkeys related to the human Kaposi's sarcoma-associated herpesvirus. J. Virol. **71**:9764–9769.
16. **Dittmer D, et al.** 1999. Experimental transmission of Kaposi's sarcoma-associated herpesvirus (KSHV/HHV-8) to SCID-hu Thy/Liv mice. J. Exp. Med. **190**:1857–1868.
17. **Estep RD, Powers MF, Yen BK, Li H, Wong SW.** 2007. Construction of an infectious rhesus rhadinovirus bacterial artificial chromosome for the analysis of Kaposi's sarcoma-associated herpesvirus-related disease development. J. Virol. **81**:2957–2969.
18. **Flowers CC, Flowers SP, Nabel GJ.** 1998. Kaposi's sarcoma-associated herpesvirus viral interferon regulatory factor confers resistance to the antiproliferative effect of interferon-alpha. Mol. Med. **4**:402–412.
19. **Fuld S, Cunningham C, Klucher K, Davison AJ, Blackbourn DJ.** 2006. Inhibition of interferon signaling by the Kaposi's sarcoma-associated herpesvirus full-length viral interferon regulatory factor 2 protein. J. Virol. **80**:3092–3097.
20. **Gao SJ, et al.** 1997. KSHV ORF K9 (vIRF) is an oncogene which inhibits the interferon signaling pathway. Oncogene **15**:1979–1985.
21. **Honda K, Taniguchi T.** 2006. IRFs: master regulators of signalling by Toll-like receptors and cytosolic pattern-recognition receptors. Nat. Rev. Immunol. **6**:644–658.
22. **Hosmer DW, Lemeshow S.** 1989. Applied logistic regression, 1st ed. John Wiley & Sons, Inc, New York, NY.
23. **Huber JP, Farrar JD.** 2011. Regulation of effector and memory T-cell functions by type I interferon. Immunology **132**:466–474.
24. **Joo CH, et al.** 2007. Inhibition of interferon regulatory factor 7 (IRF7)-mediated interferon signal transduction by the Kaposi's sarcoma-associated herpesvirus viral IRF homolog vIRF3. J. Virol. **81**:8282–8292.
25. **Kaleeba JA, Bergquam EP, Wong SW.** 1999. A rhesus macaque rhadinovirus related to Kaposi's sarcoma-associated herpesvirus/human herpesvirus 8 encodes a functional homologue of interleukin-6. J. Virol. **73**:6177–6181.
26. **Kirchoff V, Wong S, St JS, Pari GS.** 2002. Generation of a life-expanded rhesus monkey fibroblast cell line for the growth of rhesus rhadinovirus (RRV). Arch. Virol. **147**:321–333.
27. **Lagos D, et al.** 2007. Kaposi sarcoma herpesvirus-encoded vFLIP and vIRF1 regulate antigen presentation in lymphatic endothelial cells. Blood **109**:1550–1558.
28. **Lee HR, et al.** 2009. Kaposi's sarcoma-associated herpesvirus viral interferon regulatory factor 4 targets MDM2 to deregulate the p53 tumor suppressor pathway. J. Virol. **83**:6739–6747.
29. **Lubyova B, Pitha PM.** 2000. Characterization of a novel human herpesvirus 8-encoded protein, vIRF-3, that shows homology to viral and cellular interferon regulatory factors. J. Virol. **74**:8194–8201.
30. **Luft T, et al.** 1998. Type I IFNs enhance the terminal differentiation of dendritic cells. J. Immunol. **161**:1947–1953.
31. **Maurer T, Ponte M, Leslie K.** 2007. HIV-associated Kaposi's sarcoma with a high CD4 count and a low viral load. N. Engl. J. Med. **357**:1352–1353.
32. **Messaoudi I, et al.** 2009. Simian varicella virus infection of rhesus macaques recapitulates essential features of varicella zoster virus infection in humans. PLoS Pathog. **5**:e1000657.
33. **Moore PS, Boshoff C, Weiss RA, Chang Y.** 1996. Molecular mimicry of human cytokine and cytokine response pathway genes by KSHV. Science **274**:1739–1744.
34. **Nakamura H, Li M, Zarycki J, Jung JU.** 2001. Inhibition of p53 tumor suppressor by viral interferon regulatory factor. J. Virol. **75**:7572–7582.
35. **Offermann MK.** 2007. Kaposi sarcoma herpesvirus-encoded interferon regulator factors. Curr. Top. Microbiol. Immunol. **312**:185–209.
36. **Orzechowska BU, et al.** 2009. Viral interleukin-6 encoded by rhesus macaque rhadinovirus is associated with lymphoproliferative disorder (LPD). J. Med. Primatol. **38**(Suppl 1):2–7.
37. **Orzechowska BU, et al.** 2008. Rhesus macaque rhadinovirus-associated non-Hodgkin lymphoma: animal model for KSHV-associated malignancies. Blood **112**:4227–4234.
38. **Osborne J, Moore PS, Chang Y.** 1999. KSHV-encoded viral IL-6 activates multiple human IL-6 signaling pathways. Hum. Immunol. **60**:921–927.
39. **Park J, et al.** 2007. Identification of the DNA sequence interacting with Kaposi's sarcoma-associated herpesvirus viral interferon regulatory factor 1. J. Virol. **81**:12680–12684.

40. **Pica F, Volpi A.** 2007. Transmission of human herpesvirus 8: an update. Curr. Opin. Infect. Dis. **20**:152–156.
41. **Pitcher CJ, et al.** 2002. Development and homeostasis of T cell memory in rhesus macaque. J. Immunol. **168**:29–43.
42. **Renne R, et al.** 2004. Experimental transmission of Kaposi's sarcoma-associated herpesvirus (KSHV/HHV-8) to SIV-positive and SIV-negative rhesus macaques. J. Med. Primatol. **33**:1–9.
43. **Rivas C, Thlick AE, Parravicini C, Moore PS, Chang Y.** 2001. Kaposi's sarcoma-associated herpesvirus LANA2 is a B-cell-specific latent viral protein that inhibits p53. J. Virol. **75**:429–438.
44. **Robinson BA, Estep RD, Messaoudi I, Rogers KS, Wong SW.** 2011. Viral interferon regulatory factors decrease the induction of type I and type II IFN during rhesus macaque rhadinovirus infection. J. Virol. [Epub ahead of print.] doi:10.1128/JVI.05047-11.
45. **Russo JJ, et al.** 1996. Nucleotide sequence of the Kaposi sarcoma-associated herpesvirus (HHV8). Proc. Natl. Acad. Sci. U. S. A. **93**:14862–14867.
46. **Searles RP, Bergquam EP, Axthelm MK, Wong SW.** 1999. Sequence and genomic analysis of a rhesus macaque rhadinovirus with similarity to Kaposi's sarcoma-associated herpesvirus/human herpesvirus 8. J. Virol. **73**:3040–3053.
47. **Seo T, Park J, Lee D, Hwang SG, Choe J.** 2001. Viral interferon regulatory factor 1 of Kaposi's sarcoma-associated herpesvirus binds to p53 and represses p53-dependent transcription and apoptosis. J. Virol. **75**:6193–6198.
48. **Soulier J, et al.** 1995. Kaposi's sarcoma-associated herpesvirus-like DNA sequences in multicentric Castleman's disease. Blood **86**:1276–1280.
49. **Vandevenne P, Sadzot-Delvaux C, Piette J.** 2010. Innate immune response and viral interference strategies developed by human herpesviruses. Biochem. Pharmacol. **80**:1955–1972.
50. **West JA, Gregory SM, Sivaraman V, Su L, Damania B.** 2011. Activation of plasmacytoid dendritic cells by Kaposi's sarcoma-associated herpesvirus. J. Virol. **85**:895–904.
51. **White JA, Yang X, Todd PA, Lerche NW.** 2011. Longitudinal patterns of viremia and oral shedding of rhesus rhadinovirus and retroperitoneal fibromatosis herpesviruses in age-structured captive breeding populations of rhesus macaques (Macaca mulatta). Comp. Med. **61**:60–70.
52. **Wies E, et al.** 2009. The Kaposi's sarcoma-associated herpesvirus-encoded vIRF-3 inhibits cellular IRF-5. J. Biol. Chem. **284**:8525–8538.
53. **Wies E, et al.** 2008. The viral interferon-regulatory factor-3 is required for the survival of KSHV-infected primary effusion lymphoma cells. Blood **111**:320–327.
54. **Wong SW, et al.** 1999. Induction of B cell hyperplasia in simian immunodeficiency virus-infected rhesus macaques with the simian homologue of Kaposi's sarcoma-associated herpesvirus. J. Exp. Med. **190**:827–840.
55. **Zimring JC, Goodbourn S, Offermann MK.** 1998. Human herpesvirus 8 encodes an interferon regulatory factor (IRF) homolog that represses IRF-1-mediated transcription. J. Virol. **72**:701–707.